ACS Catalysis

RESEARCH ARTICLE

pubs.acs.org/acscatalysis

# Modification of Metal Nanoparticles with $TiO_2$ and Metal−Support Interaction in Photodeposition

Junya Ohyama,[†] Akira Yamamoto,[†] Kentaro Teramura,[*,‡] Tetsuya Shishido,[†] and Tsunehiro Tanaka[*,†]

[†]Department of Molecular Engineering, Graduate School of Engineering, Kyoto University, Kyoto 615-8510, Japan

[‡]Kyoto University Pioneering Research Unit for Next Generation, Kyoto University, Kyoto 615-8510, Japan

Supporting Information

**ABSTRACT:** Rh, Pt, and Au metals photodeposited on $TiO_2$ with an anatase phase (M−$TiO_2$(p), M: Rh, Pt, Au) were studied using transmission electron microscopy (TEM), scanning transmission electron microscopy, energy dispersive X-ray (EDX) analysis, X-ray absorption fine structure (XAFS) spectroscopy, X-ray photoelectron spectroscopy (XPS), and XPS depth profile analysis. The TEM images of Rh−$TiO_2$-(p) and Pt−$TiO_2$(p) did not clearly show the grain boundary of metal particles, although the Rh and Pt species of Rh−$TiO_2$(p) and Pt−$TiO_2$-(p) were observed by EDX analysis to show the metal particles 10−20 nm in size. These results suggest that the photodeposited Rh and Pt metal particles have a disorganized structure, which is also supported by extended XAFS spectral analysis. It is speculated that a strong metal−support interaction takes place in the case of Rh and Pt, resulting in the disorganized structure. In the case of Au, however, metal particles with a well-organized and spherical structure were observed, indicating that Au does not strongly interact with $TiO_2$. The XPS analyses revealed that the surface of metal particles of M−$TiO_2$(p) received electrons from $TiO_2$. The XPS depth profile analysis suggests that the metal particles are modified with $TiO_2$. $TiO_{2-\delta}$ generated by the photoirradiation of $TiO_2$ can cause the modification and the disorganized structure of Rh and Pt metal particles.

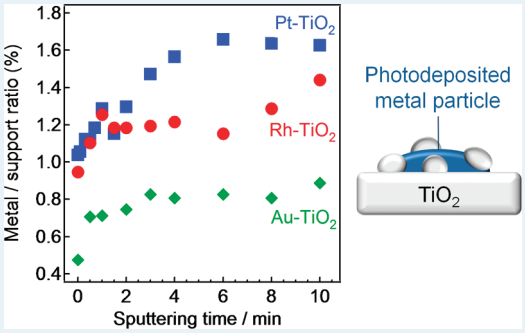


**KEYWORDS:** photodeposition, Rh−$TiO_2$, Pt−$TiO_2$, Au−$TiO_2$, M−TiO, photoirradiation, EM, EDX, XAFS, XPS, depth analysis

## INTRODUCTION

Photodeposition has been used to recover noble metals, to remove metal cations from aqueous effluents, and to prepare metal−supported catalysts and photocatalysts ever since Bard et al. reported it in 1978.[1−6] The irradiation of a semiconductor powder (e.g., $TiO_2$) with UV light results in the reduction of metal cations having appropriate redox potential by the photo-excited electrons, generating metal particles on $TiO_2$. Very recently, we reported the photodepostion process of Rh metal particles on $TiO_2$ using in situ time-resolved energy dispersive X-ray absorption fine structure spectroscopy (DXAFS).[7,8] The spectral analysis revealed that the $RhCl_3$ precursor was proportionally reduced to Rh metal particles as the photoirradiation time increased. The coordination number (CN) of the Rh−Rh pair also proportionally increased with the photoirradiation time and stopped at a CN of ∼10, although that of Rh foil is 12. These results indicate that the fine Rh metal particles with a uniform CN of a Rh−Rh pair (∼10) consistently appear. Interestingly, Rh metal particles were not identified by transmission electron microscopy (TEM) observation, although Rh domains of a few dozen nanometers were observed by energy dispersive X-ray (EDX) analysis (Figure 1). We expected that Rh metal particles prepared by the photodeposition process would have a disorganized structure. The structure can be induced by the metal−support interaction, which can inhibit the formation of Rh−Rh bonds.[9]

The interaction between the support and the metal in a supported-metal catalyst plays an important role in the catalytic reaction.[10,11] The treatment of group VIII noble metals (e.g., Pt, Rh, Pd, and Ir) on reducible oxide supports (e.g., $TiO_2$ and $Nb_2O_5$) with $H_2$ at high temperature suppresses the $H_2$ and CO chemisorptions of the metal particles. This phenomenon was termed strong metal−support interaction (SMSI). The SMSI changes the catalytic activity and selectivity of the metal particles because the SMSI influences the electronic properties and the morphology of metal particles, and causes the modification of metal particles with reduced supports (e.g., $TiO_{2-\delta}$) generated by $H_2$ treatment at high temperature.[11−15]

It is well-known that photoirradiation to $TiO_2$ generates $TiO_{2-\delta}$, which can serve as the formation site for metal particles.[16,17] As mentioned above, $TiO_{2-\delta}$ strongly interacts with metal species to change the electronic properties and morphology of those metal particles. The electronic properties of the metal particles change the Schottky barrier height between the metal and the support, affecting the efficiency of charge separation,[3] while the variation in the morphology of metal particles influences the way in which the substrates adsorb the metals. The

Received: November 7, 2010
Revised: January 18, 2011
Published: February 04, 2011

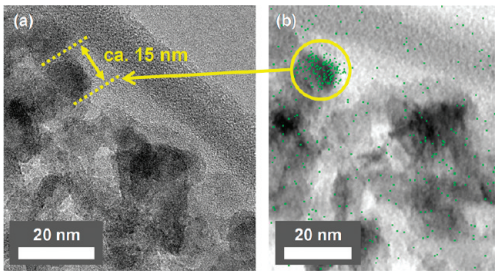


**Figure 1.** (a) TEM image and (b) overlay of EDS mapping image on STEM image of Rh−$TiO_2$(p).

efficiency of charge separation and the manner of adsorption in turn affect the photocatalytic activity. Therefore, the interaction between metal and support is an important factor for metal-modifying photocatalysts. However, there are few studies dealing with the interaction.[3,6,18]

To study the metal−supported interaction that occurs in photodeposition, we used TEM, EDX, XAFS, XPS, and depth analysis to investigate the structure and electronic properties of Rh and Pt (group VIII metals) and Au (a group IB metal) photodeposited on $TiO_2$.

## EXPERIMENTAL SECTION

**Preparation.** Photodeposition of Rh, Pt, and Au particles on $TiO_2$ was carried out in a closed batch system. As a typical photodeposition method, 500 mg of $TiO_2$ (JRC-TIO-8, anatase phase) calcined at 673 K in air was suspended in 3.2 mL of methanol in a batch reactor made of Pylex glass with a flat ceiling window for illumination, followed by addition of 0.8 mL of aqueous solution of metal precursor (0.076 mmol). $RhCl_3 \cdot H_2O$, $H_2PtCl_6 \cdot 6H_2O$, and $HAuCl_4 \cdot 4H_2O$ (Wako Pure Chemical Industries, Ltd.) were used as metal precursors. The suspension was irradiated for 120 min with a 200-W Hg−Xe lamp equipped with fiber optics, a collective lens, and a mirror (San-Ei Electric Co., Ltd., UVF-204S type C) after Ar bubbling for 10 min. The suspension was then filtered, and the residual powder was washed with 100 mL of purified water. The residue was placed in an oven at 353 K, resulting in a powder that is abbreviated M−$TiO_2$(p) (M: Rh, Pt, and Au). As a reference, Rh and Pt were deposited on $TiO_2$ by an impregnation method. The suspension consisting of each metal precursor (0.76 mmol) in 150 mL of water and $TiO_2$ (5.00 g) was stirred at 353 K for 2 h and then dried. The sample was then calcinated at 773 K for 3 h. The resulting powder was reduced under ∼100 Torr of $H_2$ at 573 and 773 K to prepare M−$TiO_2$-(i573) and M−$TiO_2$(i773) (M: Rh and Pt), respectively.

Au−$TiO_2$(dp) was also prepared by the deposition−precipitation method as a reference.[19] A NaOH aqueous solution (1 M) was added dropwise to a 200 mL $HAuCl_4$ aqueous solution (0.21 mmol) to adjust the pH of the solution to between 6 and 10. $TiO_2$ (2.03 g) was added to the solution and stirred at 343 K for 2 h, followed by filtration. The resulting residue was washed by 20-min stirring in water at 343 K, and the solution was discarded by filtration. The washing process was repeated three times. The resulting powder was dried under 353 K and then calcinated at 573 K to prepare Au−$TiO_2$(dp).

**Analysis.** TEM, STM, and EDX mapping images were obtained with a JEOL JEM-2100F transmission electron microscope operating at an accelerating voltage of 200 kV. TEM samples were prepared by depositing drops of a methanol suspension containing small amounts of the powders onto a carbon-coated copper grid (Okenshoji Co. Ltd.) and allowing the methanol to evaporate in air.

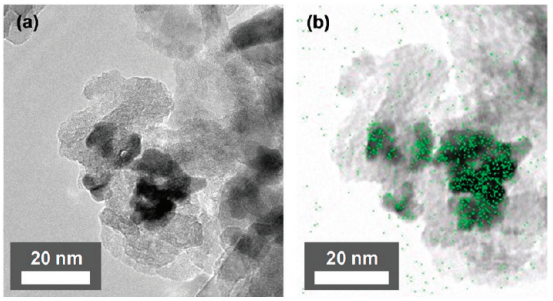


**Figure 2.** (a) TEM image and (b) overlay of EDS mapping image on STEM image of Pt−$TiO_2$(p).

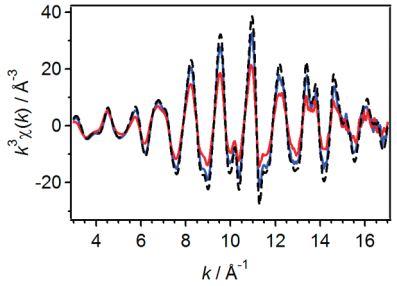


**Figure 3.** Rh K-edge $k^3$ weighted EXAFS spectra of Rh−$TiO_2$(p) (red solid line), those after heat treatment (blue solid line), and Rh foil (black dashed line).

The XAFS measurement at the Rh K-edge was carried out using an NW10A beamline of the Photon Factory Advanced Ring (PF-AR, 6.5 GeV) at the High Energy Accelerator Research Organization (KEK; Tsukuba, Japan) with a Si(311) double-crystal monochromator. Ion chambers of the I and $I_0$ detector were filled with Ar (100%) and Kr (100%) flow, respectively. The X-ray energy was calibrated with a spectrum of Rh foil. The XAFS measurement at the Au and Pt $L_3$-edge was performed using a BL7C beamline of a Photon Factory storage ring (PF, 2.5GeV). Ion chambers of the I and $I_0$ detector were filled with $N_2$ (85%)/Ar (15%) and Ar (100%) flow, respectively. The X-ray energy was calibrated with a spectrum of Cu foil at 8980 eV. The XAFS spectra of all of the samples were recorded in the transmission mode. Data reduction of XAFS spectra was performed using the REX2000 program, version 2.5.9 (Regaku Corp.). The $k^3$ weighted Rh K-edge and Pt $L_3$-edge EXAFS oscillations were Fourier-transformed in the ranges of 3.2−17.0 and 3.1−16.9 Å$^{-1}$, respectively. The curve-fitting of Fourier-filtered EXAFS spectra was performed using empirical parameters extracted from the XAFS spectrum of the Rh and Pt foils.

XPS spectra were acquired using an ULVAC PHI 5500MT system. Samples mounted on indium foil were analyzed using Mg $K\alpha_{1,2}$ radiation (15 kV, 400 W) in a chamber with the gas pressure less than $1 \times 10^{-8}$ Torr. The electron takeoff angle was set at 45°. Binding energies were referenced to C 1s peak of residual carbon at 284.6 eV. Sputtering was performed by a Xe ion beam (3.0 kV) with raster size 1.1 mm × 2.1 mm.

## RESULT AND DISCUSSION

**Structural Analysis.** Figure 1 shows the TEM image and the overlay of the EDX mapping image on the STEM image of


dx.doi.org/10.1021/cs100072k |*ACS Catal.* 2011, 1, 187–192

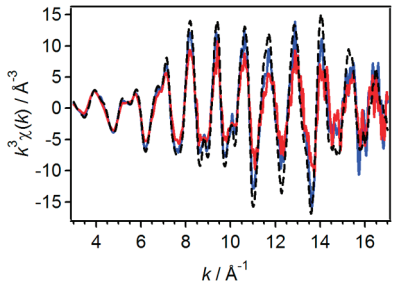


**Figure 4.** Pt $L_3$-edge $k^3$ weighted EXAFS spectra of Pt−$TiO_2$(p) (red solid line), those after heat treatment (blue solid line), and Pt foil (black dashed line).

**Table 1. Curve-Fitting Results of Rh−Rh Scattering of Rh Metal Particles and Pt−Pt Scattering of Pt Metal Particles Prepared by the Photodeposition**[a]

| | CN[b] | $r$/Å[c] | $\sigma$/Å[d] | $R$ (%)[e] |
|---|---|---|---|---|
| Rh | 9.0 | 2.69 | 0.069 | 21.2 |
| Pt | 10.1 | 2.76 | 0.072 | 23.8 |

[a] Rh: R fitting range is 2.00−2.76 Å, and $k$ fitting range is 4.6−16.4 Å$^{-1}$. Pt: R fitting range is 2.30−3.03 Å, and $k$ fitting range is 4.6−16.2 Å$^{-1}$. [b] CN, coordination number. [c] $r$, interatomic distance. [d] $\sigma$, Debye−Waller factor. [e] So-called $R$ factor.

Rh−$TiO_2$(p). The particle boundaries of the Rh metal species are not identified in the TEM image, although the existence of an Rh metal species is identified as green dots that have a domain width of ∼15 nm. As a reference, the TEM image of Rh−$TiO_2$ (i573) clearly showed Rh metal particles ∼2 nm in diameter. Figure 2 shows the TEM image and the overlay of the EDX mapping image on the STEM image of Pt−$TiO_2$(p). The metal species of Pt−$TiO_2$(p) and Rh−$TiO_2$(p) are identified in the EDX mapping images but not in the TEM images. Rh and Pt particles that have a disordered structure on $TiO_2$ show ambiguous contrast, Moire fringes, and particle boundaries.

Figures 3 and 4 show the Rh K-edge and Pt $L_3$-edge with $k^3$ weighted EXAFS spectra of Rh−$TiO_2$(p) and Pt−$TiO_2$(p). These EXAFS spectra have the same phase as the respective foils and a smaller oscillation amplitude than the respective foils. The small amplitude is indicative of the small number of metal−metal pairs. Table 1 lists the structural parameters obtained by the curve fitting of the Fourier-transformed EXAFS spectra of Rh−$TiO_2$(p) and Pt−$TiO_2$(p). The CNs of the Rh and Pt metal particles are 9.0 and 10.1, respectively, although the foils have a CN of 12. This suggests the formation of metal particles of ca. 2−3 nm diameter, assuming the cuboctahedral structure. The agglomerates of these small metal particles would be observed in the EDS mapping images to show a metal domain ∼15 nm. Our previous work indicated that such metal particles consistently appear with an increase in photoirradiation time.[7,8] It is likely that the small metal particles aggregate and form the large particles with ∼15 nm, as observed by the EDS analysis.

Au−$TiO_2$(p) was also observed by TEM, as shown in Figure 5. The Au metal particles show clear particle boundaries and a spherical structure. This means a well-organized structure for the Au metal particles. Figure 6 exhibits the Au $L_3$-edge $k^3$ weighted EXAFS spectra of Au−$TiO_2$(p). The EXAFS spectrum of Au−$TiO_2$(p) has almost the same amplitude as the Au foil, which supports the well-organized structure of Au metal particles indicated by the TEM analysis.

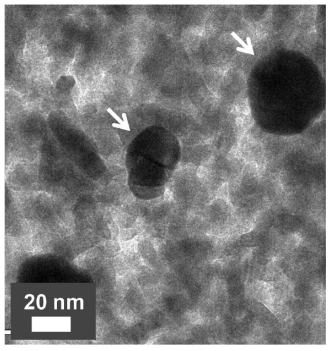


**Figure 5.** TEM image of Au−$TiO_2$(p).

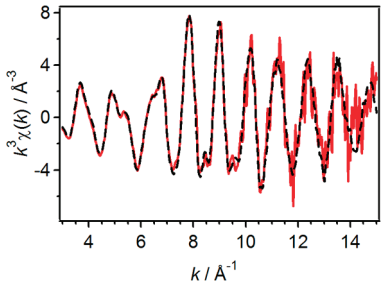


**Figure 6.** Au $L_3$-edge $k^3$ weighted EXAFS spectra of Au−$TiO_2$(p) (red solid line) and Au foil (black dashed line).

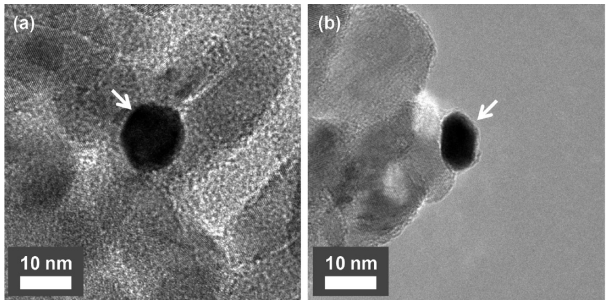


**Figure 7.** TEM images of (a) Rh−$TiO_2$(p) and (b) Pt−$TiO_2$(p) after heat treatment at 673 K under vacuum.

The structure of the metal particles is different among the different kinds of metals. This is due to the difference in the strength of the metal−support interaction between the kinds of metals: the strong interaction of Rh and Pt metal particles with $TiO_2$ causes their disorganized structure, whereas the weak interaction of Au metal particles results in the spherical and well-organized structure.[20,21] In fact, as mentioned above, Rh and Pt are active metals for SMSI, but Au is not. It is also noteworthy that the disorganized structures of Rh and Pt metal particles of Rh−$TiO_2$(p) and Pt−$TiO_2$(p) vary according to the heat treatment at 673 K to show spherical particles with obvious boundaries, as shown in Figure 7. The change in structure is also observed by the EXAFS spectra as the increase of the oscillation amplitude (Figures 3 and 4). Metal−metal bonds are probably formed beyond the metal−support interaction by the heat treatment. Therefore, the disorganized structure of Rh and Pt metal particles are produced after the photodeposition without calcination.

**Analysis of Electronic Properties.** Figure 8 shows the Rh 3d XPS. The electronic properties of the surfaces of metal particles were evaluated using the peak energy of Rh $3d_{5/2}$ XPS. The lower


dx.doi.org/10.1021/cs100072k |ACS Catal. 2011, 1, 187–192

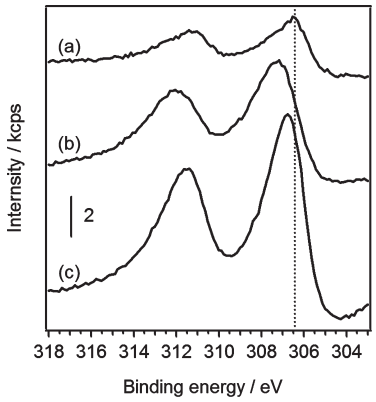


**Figure 8.** Rh 3d XPS spectra of (a) Rh−$TiO_2$(p), (b) Rh−$TiO_2$(i573), and (c) Rh−$TiO_2$(i773). The dashed line shows the energy at the Rh $3d_{5/2}$ peak of Rh−$TiO_2$(p).

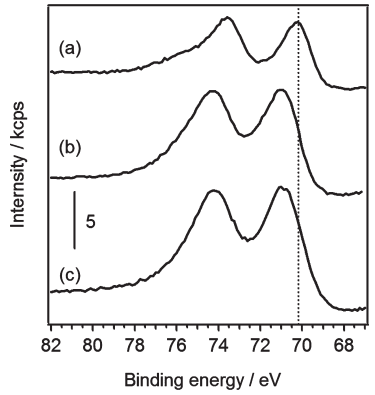


**Figure 9.** Pt 4f XPS spectra of (a) Pt−$TiO_2$(p), (b) Pt−$TiO_2$(i573), and (c) Pt−$TiO_2$(i773). The dashed line shows the energy at the Pt $4f_{7/2}$ peak of Pt−$TiO_2$(p).

energy at the peak indicates the more electron-rich surface of metal particles. The peak of Rh $3d_{5/2}$ XPS of Rh−$TiO_2$(p) appears at 306.5 eV (Figure 8a), which is of lower energy than that of Rh foil at 307.0 eV.[22] This indicates that the surface of Rh metal particles of Rh−$TiO_2$(p) sample is more electron-rich than Rh foil.

As controls, Rh−$TiO_2$(i773) and Rh−$TiO_2$(i573) (which are and are not in SMSI state, respectively) were also analyzed by XPS (Figure 8b and c). The XPS peak of Rh−$TiO_2$(i773) (306.8 eV) presents at lower energy than that of Rh−$TiO_2$(i573) (307.2 eV), which indicates that the surface of Rh metal particles of Rh−$TiO_2$(i773) have more electrons than that of Rh−$TiO_2$-(i573). This is probably due to the SMSI effect.[23,24] The peak energy of Rh−$TiO_2$(p) being lower than Rh−$TiO_2$(i773) suggests that the Rh metal particles of Rh−$TiO_2$(p) have a stronger interaction with $TiO_2$ than those of Rh−$TiO_2$(i773).

Figure 9 represents the Pt 4f XPS. The peak of Pt $4f_{7/2}$ of Pt−$TiO_2$(p) appears at a lower binding energy (70.2 eV) than that of the references (Pt−$TiO_2$(i573), 70.9 eV; Pt−$TiO_2$-(i773), 71.0 eV; Pt foil, 70.9 eV).[22] Only the Pt metal particles of Pt−$TiO_2$(p) are electron-rich. Not only Rh but also Pt metal particles interact more strongly with $TiO_2$ to obtain more electrons from the $TiO_2$ than those reduced by $H_2$ at the high temperature. The ideal condition for SMSI may thus be provided in the photodeposition process.

Figure 10 shows the Au 4f XPS of Au−$TiO_2$(p), together with those of Au−$TiO_2$(dp) and Au foil as references. The peak of Au

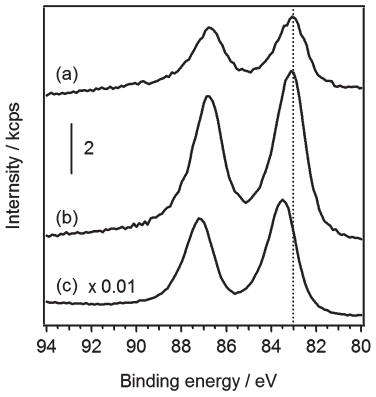


**Figure 10.** Au 4f XPS spectra of (a) Au−$TiO_2$(p), (b) Au−$TiO_2$(dp), (c) Au foil. The dashed line shows the energy at the Au $4f_{7/2}$ peak of Au−$TiO_2$(p).

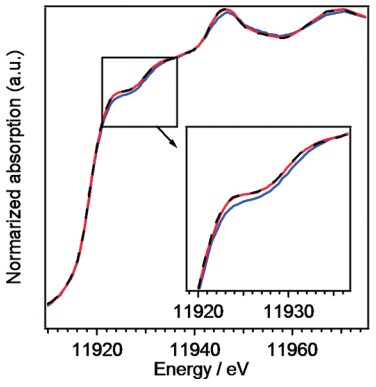


**Figure 11.** Au $L_3$-edge XANES spectra of Au−$TiO_2$(p) (red solid line), Au−$TiO_2$(dp) (blue solid line), and Au foils (black dashed line).

$4f_{7/2}$ XPS of Au−$TiO_2$(p) appears at a lower binding energy (83.1 eV) than that of Au foil (83.5 eV) and at the same energy as that of Au−$TiO_2$(dp). This indicates that the surface electronic property of Au−$TiO_2$(p) is the same as that of Au−$TiO_2$(dp) and is more negative than that of Au foil.

Figure 11 exhibits Au $L_3$-edge X-ray absorption near the edge structure (XANES) spectra of Au−$TiO_2$(p), Au−$TiO_2$(dp), and Au foil. We can evaluate the mean electronic properties of Au metal particles from the peak at the edge, the so-called white line. The white line at the Au $L_3$-edge is attributed to the electron transition from the $2p_{3/2}$ to the 5d state. The white line of Au−$TiO_2$(p) has a slightly greater intensity than that of Au−$TiO_2$(dp) and is the same as that of Au foil. This result indicates that the 5d state of Au atoms in Au−$TiO_2$(p) has more holes than those in Au−$TiO_2$(dp) and is the same as that of Au foil.[25] In other words, all of the Au atoms in Au−$TiO_2$(p) are more electron-poor than those in Au−$TiO_2$(dp) but are in the same state as those of the Au foil. However, the XPS analysis indicates that the surface electronic properties of Au−$TiO_2$(p) are the same as those of Au−$TiO_2$(dp). It is concluded that only the surface of Au metal particles of Au−$TiO_2$(p) is as electron-rich as that of Au−$TiO_2$-(dp). On the other hand, Au metal particles of Au−$TiO_2$(p) are much larger (∼20−40 nm) than those of Au−$TiO_2$(dp) (∼3 nm, determined by a TEM observation). The Au metal particles of Au−$TiO_2$(p) should therefore be modified with $TiO_2$ to have the same surface electronic properties as the much smaller Au metal particles of Au−$TiO_2$(dp).


dx.doi.org/10.1021/cs100072k |*ACS Catal.* 2011, 1, 187–192

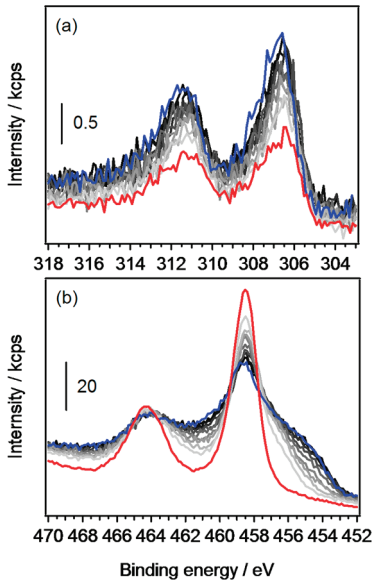


**Figure 12.** Series of (a) Rh 3d and (b) Ti 2p XPS spectra of Rh−$TiO_2$(p) during sputtering with Xe ion for 10 min. The spectra change from red (0 min) to blue (10 min).

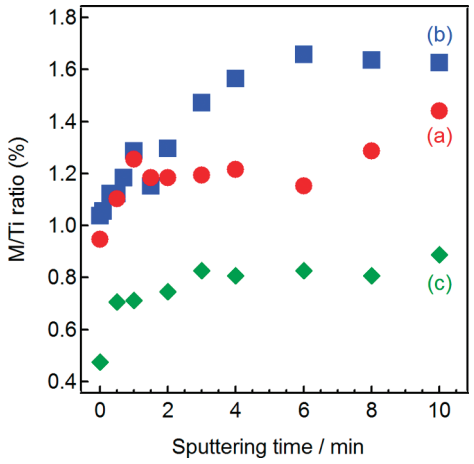


**Figure 13.** The change in M/Ti ratio of M−$TiO_2$(p) (M: (a) Rh, (b) Pt, (c) Au) by Xe sputtering for 10 min.

**Depth Analysis.** Figure 12 shows the change in Rh 3d and Ti 2p XPS spectra of Rh−$TiO_2$(p) by Xe ion sputtering. The peak intensity of the Rh 3d XPS spectrum increased with sputtering time. With greater sputtering, the two bands of Ti 2p XPS become smaller and broader in the lower-energy side. This change is due to the reduction of $TiO_2$ by Xe ion sputtering. The composition ratio between Rh and Ti (Rh/Ti ratio) at a given sputtering time was evaluated from those peak areas divided by respective atomic sensitivity factors.[22] Figure 13a shows the variation in Rh/Ti ratio with sputtering time of Rh−$TiO_2$(p). The Rh/Ti ratio of Rh−$TiO_2$(p) increased as the sputtering time increased, approaching 1.4% after 10 min of sputtering. The two models of Rh−$TiO_2$(p) are assumed from the depth profile.[26] One is that Rh metal particles having a size comparable to $TiO_2$ particles are modified with $TiO_2$. The other is that the Rh species is intermixed with a $TiO_2$ particle. The EDX analysis reveals that the Rh metal particles have almost the same size as that of $TiO_2$ (~15 nm), which is in accordance with the first model. The depth analyses of Pt−$TiO_2$(p) and Au−$TiO_2$(p) were also performed as shown in Figure 13b and c. The M/Ti ratio (M: Pt, Au) increased as the sputtering time increased as well as Rh/Ti ratio of Rh−$TiO_2$(p) (Figure 13a). In addition, Pt and Au metal particles have a size comparable to $TiO_2$, as shown in the TEM images. It is concluded that the photodeposited metal (Rh, Pt, and Au) particles having almost the same size as $TiO_2$ particles are modified with $TiO_2$.

**Mechanisms of SMSI and Photodeposition.** $TiO_{2-\delta}$ is well-known as a key species in SMSI and in the surface modification of metal particles.[11] $TiO_{2-\delta}$ can be also generated during photodeposition by the consumption of the photogenerated holes on $O^{\delta+}$ of $TiO_2$ without any reduction on $Ti^{\delta-}$.[27] In addition, $TiO_{2-\delta}$ originally exists on the surface of $TiO_2$ as defect sites. $Ti^{3+}$ in $TiO_{2-\delta}$ contributes to an electron trap under the conduction band of $TiO_2$, leading to a flow of excited electrons to $TiO_{2-\delta}$[28] and a reduction of metal ions on $TiO_{2-\delta}$. In fact, the defect sites were proposed as the active sites for formation of metal particles in the photodeposition process.[16,17] Therefore, $TiO_{2-\delta}$ can influence the photodeposition.

As described above, we reported the photodeposition process of Rh metal particles. Rh metal particles do not grow in increments, but Rh metal particles having a CN of ~10 for the Rh−Rh pair appear consistently.[7] The CN of the Rh−Rh pair indicates the formation of particles with ~2−3 nm, assuming the cuboctahedral structure. In this study, we proposed that the Rh metal particles strongly interact with, and are modified by their interaction with, $TiO_2$ (more specifically, with $TiO_{2-\delta}$).

In addition, the formation of the disordered structure of Rh metal particles having ~15 nm of domain is indicated. From these results, we now assume that Rh metal particles having ~2−3 nm constantly appear and aggregate to form a disordered structure, not a spherical and well-ordered structure, as is the case with Au, due to the strong metal−support interaction and modification with $TiO_2$. Pt metal particles are probably formed in the same manner as Rh metal particles because Pt−$TiO_2$(p) shows the same behavior as Rh−$TiO_2$(p). On the other hand, in the case of Au, metal particles will grow in increments by aggregation to form large spherical particles, because Au does not have a strong interaction with $TiO_2$ in comparison with Rh and Pt.[17,29]

In this study, it is suggested that metal particles are modified with $TiO_2$ in the photodeposition process, regardless of the kind of metal. $TiO_{2-\delta}$ may migrate onto metal particles, or a metal precursor may be reduced in the oxygen vacancy site of $TiO_{2-\delta}$ to form metal particles in $TiO_{2-\delta}$. On the other hand, Pt−$TiO_2$(p) and Pt−$TiO_2$(i773K) were tested for hydrogenation of ethylene (see the Supporting Information). As a result, ethylene was smoothly converted to ethane on Pt−$TiO_2$(p); however, ethylene was hardly hydrogenated on Pt−$TiO_2$(i773K). It is speculated that the metal particles prepared by photodeposition are not encapsulated but are partially modified with $TiO_2$, in other words, decorated by $TiO_2$; however, the metal particles are encapsulated by high-temperature reduction with $H_2$. The heat condition may be essential for migration of $TiO_2$ to encapsulate the metal particles.

## CONCLUSIONS

When Rh, Pt, and Au metal particles were photodeposited on $TiO_2$, the Rh and Pt metal particles showed a disorganized structure. On the other hand, Au metal particles showed a well


dx.doi.org/10.1021/cs100072k |ACS Catal. 2011, 1, 187–192

organized and spherical structure. The difference in structure between these metals is due to the difference in the strength of metal−support interaction: Rh and Pt strongly interact with $TiO_2$ and Au does not. These metal particles were partially covered by $TiO_2$ (more specifically, $TiO_{2-\delta}$), which provides electrons to the surface of metal particles.

## ■ ASSOCIATED CONTENT

**Supporting Information.** Additional information as noted in the text. This material is available free of charge via the Internet at http://pubs.acs.org.

## ■ AUTHOR INFORMATION

### Corresponding Author

*(K.T.) Phone: +81-75-585-6095. Fax: +81-75-585-6096. E-mail: kentaro.teramura@kupru.iae.kyoto-u.ac.jp. (T.T.) Phone: +81-75-383-2558. Fax: +81-75-383-2561. E-mail: tanakat@moleng.kyoto-u.ac.jp.

## ■ ACKNOWLEDGMENT

This study was supported by the Program for Improvement of Research Environment for Young Researchers from Special Coordination Funds for Promoting Science and Technology commissioned by the Ministry of Education, Culture, Sports, Science and Technology of Japan. T.T. acknowledges a Grant-in-Aid for Scientific Research for (B) (General) (No. 10002772) under the Ministry of Education, Culture, Sports Science and Technology of Japan. J.O. is supported by JSPS Research Fellowships for Young Scientists. The XAFS measurement was carried out by the approval of the Photon Factory Program Advisory Committee (Proposals Nos. 2008G123 and 2009G189).

## ■ REFERENCES

(1) Kraeutler, B.; Bard, A. J. *J. Am. Chem. Soc.* **1978**, *100*, 4317.
(2) Bamwenda, G. R.; Tsubota, S.; Nakamura, T.; Haruta, M. *Catal. Lett.* **1997**, *44*, 83.
(3) Wang, X. C.; Yu, J. C.; Yip, H. Y.; Wu, L.; Wong, P. K.; Lai, S. Y. *Chem.—Eur. J.* **2005**, *11*, 2997.
(4) Sato, S. *J. Catal.* **1985**, *92*, 11.
(5) Maeda, K.; Teramura, K.; Lu, D. L.; Saito, N.; Inoue, Y.; Domen, K. *Angew. Chem., Int. Ed.* **2006**, *45*, 7806.
(6) Lin, C. H.; Chao, J. H.; Liu, C. H.; Chang, J. C.; Wang, F. C. *Langmuir* **2008**, *24*, 9907.
(7) Teramura, K.; Okuoka, S.-i.; Yamazoe, S.; Kato, K.; Shishido, T.; Tanaka, T. *J. Phys. Chem. C* **2008**, *112*, 8495.
(8) Ohyama, J.; Teramura, K.; Okuoka, S.-i.; Yamazoe, S.; Kato, K.; Shishido, T.; Tanaka, T. *Langmuir* **2010**, *26*, 13907.
(9) Gonzalez-DelaCruz, V. M.; Holgado, J. P.; Pereniguez, R.; Caballero, A. *J. Catal.* **2008**, *257*, 307.
(10) Tauster, S. J.; Fung, S. C.; Garten, R. L. *J. Am. Chem. Soc.* **1978**, *100*, 170.
(11) Tauster, S. J.; Fung, S. C.; Baker, R. T. K.; Horsley, J. A. *Science* **1981**, *211*, 1121.
(12) Tauster, S. J.; Fung, S. C.; Garten, R. L. *J. Am. Chem. Soc.* **1978**, *100*, 170.
(13) Fung, S. C. *J. Catal.* **1982**, *76*, 225.
(14) Baker, R. T. K.; Prestridge, E. B.; Garten, R. L. *J. Catal.* **1979**, *59*, 293.
(15) Fu, Q.; Wagner, T.; Olliges, S.; Carstanjen, H. D. *J. Phys. Chem. B* **2005**, *109*, 944.
(16) Kowalska, E.; Abe, R.; Ohtani, B. *Chem. Commun.* **2009**, 241.
(17) Wahlstrom, E.; Lopez, N.; Schaub, R.; Thostrup, P.; Ronnau, A.; Africh, C.; Legsgaard, E.; Norskov, J. K.; Besenbacher, F. *Phys. Rev. Lett.* **2003**, *90*, 026101.
(18) Fernandez, A.; Gonzalez-Elipe, A. R.; Caballero, A.; Munuera, G. *J. Phys. Chem.* **1993**, *97*, 3350.
(19) Calla, J. T.; Bore, M. T.; Datye, A. K.; Davis, R. J. *J. Catal.* **2006**, *238*, 458.
(20) Dassenoy, F.; Philippot, K.; Ould-Ely, T.; Amiens, C.; Lecante, P.; Snoeck, E.; Mosset, A.; Casanove, M. J.; Chaudret, B. *New J. Chem.* **1998**, *22*, 703.
(21) Chakroune, N.; Viau, G.; Ammar, S.; Poul, L.; Veautier, D.; Chehimi, M. M.; Mangeney, C.; Villain, F.; Fievet, F. *Langmuir* **2005**, *21*, 6788.
(22) Wagner, C. D.; Ringgs, W. M., Davis, L. E., Moulder, J. F. *Handbook of X-ray Photoelectron Spectroscopy*; Perkin-Elmer Corp.: Eden Prairie, MN, 1979.
(23) Kao, C.-C.; Tsai, S.-C.; Chung, Y.-W. *J. Catal.* **1982**, *73*, 136.
(24) Horsley, J. A. *J. Am. Chem. Soc.* **1979**, *101*, 2870.
(25) Zhang, P.; Sham, T. K. *Appl. Phys. Lett.* **2002**, *81*, 736.
(26) Linsmeier, C.; Knozinger, H.; Taglauer, E. *Nucl. Instrum. Methods B* **1996**, *118*, 533.
(27) Takeuchi, M.; Deguchi, J.; Sakai, S.; Anpo, M. *Appl. Catal., B* **2010**, *96*, 218.
(28) Thompson, T. L.; Yates, J. T. *Chem. Rev.* **2006**, *106*, 4428.
(29) Fernandez, A.; Caballero, A.; Gonzalez-Elipe, A. R.; Herrmann, J.-M.; Dexpert, H.; Villain, F. *J. Phys. Chem.* **1995**, *99*, 3303.